# Influence of systematic errors in reference states on image quality and on stability of derived information for dc optical imaging

Yaling Pei, Harry L. Graber, and Randall L. Barbour

Optical measurements of tissue can be performed in discrete, time-averaged, and time-varying data collection modes. This information can be evaluated to yield estimates of either absolute optical coefficient values or some relative change in these values compared with a defined state. In the case of time-varying data, additional analysis can be applied to define various dynamic features. Here we have explored the accuracy with which such information can be recovered from dense scattering media using linear perturbation theory, as a function of the accuracy of the reference medium that serves as the initial guess. Within the framework of diffusion theory and a first-order solution, we have observed the following inequality regarding the sensitivity of computed measures to inaccuracy in the reference medium: Absolute measures $\gg$ relative measures $>$ dynamic measures. In fact, the fidelity of derived dynamic measures was striking; we observed that accurate measures of dynamic behavior could be defined even if the quality of the image data from which these measures were derived was comparatively modest. In other studies we identified inaccuracy in the estimates of the reference detector values, and *not* to corresponding errors in the image operators, as the primary factor responsible for instability of absolute measures. The significance of these findings for practical imaging studies of tissue is discussed.

*OCIS codes:* 100.2960, 100.2980, 170.3880, 170.4730, 170.5380.

## 1. Introduction

An unresolved issue in optical imaging of tissue is a clear appreciation of just what types of information can be obtained, and with what reliability. In principle, model-based reconstruction methods are capable of providing quantitative measures of tissue absorption and scattering coefficients. As a practical matter, however, the accuracy and reliability of this information can be expected to depend strongly on both the algorithm used for image recovery and the approach taken for data collection. Each of these domains includes a host of adjustable parameters, the optimal values of which frequently are not independent of choices made in addressing the other.

Y. Pei is with NIRx Medical Technologies Corporation, 15 Cherry Lane, Glen Head, New York 11545. H. L. Graber and R. L. Barbour (rbarbour@downstate.edu) are with the Downstate Medical Center, State University of New York, Box 25, 450 Clarkson Avenue, Brooklyn, New York 11203.

Received 19 December 2000; revised manuscript received 29 May 2001.

0003-6935/01/315755-15$15.00/0


A challenge in developing practical methods is to identify suitable trade-offs that confer stability on the overall collection and recovery process, while still providing useful information. An example of this dependency is the practical difficulties that attend the performing of contact-based optical measurements on tissue. Confounding factors include the natural plasticity of tissue, which can deform upon probe contact; its variable size; the mainly arbitrary geometry and composition of a tissue structure; the inherent vascular reactivity of tissue; and uncertainty stemming from the expected variable coupling efficiency of light at the tissue surface. Apart from presenting problems for data collection, the uncertainties that accompany these conditions can also adversely affect the reliability of derived imaging information. This is especially true when reconstruction methods are used. It is worth emphasizing that, unlike analytical measuring techniques that provide direct quantitative information about a particular parameter, image reconstruction is an indirect method that, not infrequently, is limited to providing qualitative measures of one form or another.

Among the various approaches proposed for image

recovery, commonly used are perturbation methods applied in either the Born or the Rytov approximations.[1–3] It is well appreciated that the accuracy of imaging data derived with such methods depends strongly on the use of a sufficiently accurate reference medium that serves as the initial guess.[4] While this sensitivity is not equivalent for the two approximations, with the Rytov formulation usually less sensitive,[5] a strong dependence nevertheless is observed for both. An accurate reference is one that closely matches the external geometry of the target medium, has the same size, has nearly the same internal composition, and for which the actual locations of the measuring probes and their efficiency coincide well with those modeled. While such conditions are easily met in numerical studies, they represent a much greater challenge in the case of tissue studies.

In recognition of these concerns, we have recently sought to identify alternative measurement and analysis schemes that are better suited to dealing with such uncertainties. Motivating our approach has been an appreciation that relative measures often can be made with much greater reliability than can absolute measures. The former can take on many forms, depending on the intended application. A domain we have recently emphasized,[6–8] and one commonly investigated in other fields,[9–11] is time-varying states. Typically the goal of such measures is to define the dynamics of a particular parameter, rather than to quantify the level of the parameter itself. Because features of dynamic states are often independent of the amplitude of the measured signal, data in the form of relative measures frequently reveal the desired feature without loss of information. In the case of optical imaging methods, we believe that dynamic measures, should they prove reliable, can provide fundamental new insights into a range of physiological states and disease processes. This consideration is based, in part, on appreciation that vascular reactivity, which is closely tied to tissue function and the influence of central control mechanisms, exhibits a structure-dependent frequency response. For instance, the cardiac frequency is restricted mainly to arterial structures, while the vasomotor and respiratory signals are limited mainly to the microvessels and venous side of the vascular tree, respectively. It follows that detection of these signals in a cross-sectional view from analysis of dynamic imaging data should allow for identification of different components of the vascular tree. In addition, since it is evident that vascular reactivity is coordinated, measures of its temporal correlations within an image could also provide new insights regarding modulation of tissue–vascular coupling. Insight at an even more fundamental level might also be possible from characterization of the known nonlinear, or even chaotic, properties of vascular dynamics.

Recently we have described experimental systems that are well suited to monitor the dynamic state of the vasculature in large tissue structures by use of optical imaging methods.[8,12,13] Using this instrumentation, we have, in preliminary studies on the human forearm, made observations that support our ability to detect the above-mentioned vascular responses. These include evidence of nonlinear chaotic dynamics in the vascular response,[14] spontaneous[15] or induced[16] beat frequencies that coincide with the correct anatomical structures, and confirmation of the expected vascular response following an autonomically mediated peripheral vascular stimulus (e.g., a cold shock[17]). Throughout these and related[6–8] investigations, two anecdotal observations that we consistently made were that (i) dynamic measures can be extracted with remarkable accuracy from image data whose quality is, comparatively speaking, considerably more modest and (ii), unlike efforts to define absolute optical coefficient values, the quality of image data based on relative measures, and the dynamic features derived therefrom, depend only weakly on the specifics of the reference medium chosen. Thus it appears that there may well be considerable differences in the reliability of the types of information derivable from imaging data generated with perturbation methods.

For the present study, we have systematically extended these observations and, in particular, have examined the dependence of derived information on the reference medium chosen as the initial guess. The findings obtained confirm and amplify our initial observations and also provide an explanation for the origin of the instability of reconstructed images of absolute coefficient values.

## 2. Theory

A common approach used in optical tomography is to cast the inverse problem as a linear perturbation equation. As it is most typically applied to optical imaging of tissue, the perturbation formulation relates the difference between a measured and a predicted optical signal level at the surface to the difference between coefficient values of the true target and a specified reference medium, weighted by a set of proportionality coefficients whose values depend on, among other things, the source–detector configuration and the optical properties of the medium. In practice, tomographic measurements consider some array of measurement data, thus forming a system of linear equations having the form

$$\mathbf{u} - \mathbf{u}_r = \delta\mathbf{u} = \mathbf{W}_r\delta\mathbf{x}, \tag{1}$$

where $\delta\mathbf{u}$ is the vector of differences between a set of measured light intensities ($\mathbf{u}$) and those predicted for a selected reference medium ($\mathbf{u}_r$), $\mathbf{W}_r$ is the Jacobian operator, and $\delta\mathbf{x}$ is the position-dependent difference between one or more optical properties of the target and reference media (i.e., the change in absorption coefficient $\delta\mu_a$ and the diffusion coefficient $\delta D$, where $D = 1/[3(\mu_a + \mu_s')]$ and $\mu_s'$ is the reduced scattering coefficient). The operator, referred to as the weight matrix, has coefficient values that physically represent the fractional change in light intensity at the surface caused by an incremental change in the op-

tical properties at a specified point in the medium. Mathematically this is represented by the partial differential operator $\partial u_i/\partial x_j$, where $i$ refers to the $i$th source–detector pair at the surface of the medium and $j$ to the $j$th pixel or element in the medium.

Although the perturbation equation in Eq. (1) can be solved with any of a number of available inversion schemes,[18] the accuracy and reliability of the results obtained can be greatly limited by many factors, including (but not limited to) uncertainties and errors associated with the quality of the measurement data, inaccuracies in the physical model describing light propagation in tissue, specification of an insufficiently accurate reference state, the existence of an inherently underdetermined state caused by insufficiently dense measurement sets, and weak spatial gradients in the weight function. One approach that we have taken to minimize the influence of these uncertainties has been to evaluate relative measures. The perturbation equation, expressed in the Born approximation, that relates such measures to the fractional change in coefficient values can be written as

$$\left[\frac{(\mathbf{u}_1)_i - (\mathbf{u}_2)_i}{(\mathbf{u}_2)_i}\right](\mathbf{u}_r)_i = \sum_j (\mathbf{W}_r)_{ij}(\delta\mathbf{x})_j, \qquad (2)$$

where $(\mathbf{u}_1)_i$ and $(\mathbf{u}_2)_i$ represent any two measures of interest acquired by the $i$th source–detector pair and $(\mathbf{u}_r)_i$ and $(\mathbf{W}_r)_{ij}$ are the previously described quantities computed from the reference medium; the summation in the right-hand side of Eq. (2) is over all area or volume elements considered by the image-reconstruction algorithm. Examples of such measures could include those made before and after administration of a contrast agent or, of interest to us, measurements at a specified time point compared with the temporal mean value. Just as when using Eq. (1), we assume that the relative change in the detector values is small. A corresponding expression can be written in the Rytov approximation, in which case the natural logarithm of the ratio of $(\mathbf{u}_1)_i$ to $(\mathbf{u}_2)_i$ is substituted for the bracketed quantity on the left-hand side of Eq. (2). Note that in the limit where $(\mathbf{u}_2)_i = (\mathbf{u}_r)_i$, Eq. (2) reverts to Eq. (1). As will be demonstrated, however, this is *not* a necessary condition for recovery of accurate measures of dynamic states or for obtaining qualitatively correct images or feature maps. The equivalent matrix expression for Eq. (2), relating all source–detector pairs to the medium properties, is

$$(\mathbf{D}_{\mathbf{u}_1}\mathbf{D}_{\mathbf{u}_2}^{-1} - \mathbf{I})\mathbf{u}_r = \mathbf{W}_r\delta\mathbf{x}, \qquad (3)$$

where $\mathbf{I}$ is the identity matrix [i.e., $(\mathbf{I})_{ii} = 1$, $(\mathbf{I})_{i[j\neq i]} = 0$], and the diagonal matrix $\mathbf{D}_\mathbf{v}$ for any given vector $\mathbf{v}$ is defined by $(\mathbf{D}_\mathbf{v})_{ii} \equiv v_i$, $(\mathbf{D}_\mathbf{v})_{i[j\neq i]} \equiv 0$. Formally, multiplying out the left-hand side of Eq. (3) and rearranging gives

$$\delta\mathbf{x} = \mathbf{W}_r^{-1}(\mathbf{u}_1 - \mathbf{u}_r) + \mathbf{W}_r^{-1}(\mathbf{D}_{\mathbf{u}_r}\mathbf{D}_{\mathbf{u}_2}^{-1} - \mathbf{I})\mathbf{u}_1, \qquad (4)$$

where $\mathbf{W}_r^{-1}$ is the appropriate inverse or pseudoinverse for the linear system under consideration. We refer to this formulation as the normalized difference method (NDM). Note that the first term on the right-hand side of Eq. (4) is the solution that would be obtained by solving the system $\mathbf{u}_1 - \mathbf{u}_r = \mathbf{W}_r\delta\mathbf{x}$, i.e., the standard perturbation equation. The second term amounts to a correction factor whose value is a function of the accuracy of the selected reference medium.

It is well appreciated that linear perturbation formulations are sensitive to the latter and that a sufficiently inaccurate initial guess can lead to a poor solution or even divergence. Significantly, we have demonstrated that the correction factor provides for a solution that can render an ordinarily grossly inaccurate map, provided by the first term on the right-hand side of Eq. (4), to one that, while not equal to the true solution, is proportional to it throughout the cross section. As will be shown, this allows us to compute, among other things, images reflecting temporal variations in optical properties that occur in a dense scattering medium with remarkable fidelity, even when the estimated background optical properties of the reference medium differ from those of the true target background by a factor of more than $\pm 3$. It is worth emphasizing that Eq. (3) can readily provide for solutions that simultaneously compute perturbations in absorption and scattering (diffusion) coefficients (see below) and that are updateable with iterative methods.[19]

## 3. Methods

### A. Target Media Examined

Figure 1 shows a schematic of the test medium geometry explored. In all cases, the diameter was 8 cm and there were two inclusions embedded in a homogeneous background. Each inclusion had a diameter of 1 cm, and the pair was positioned symmetrically about the center, with a separation distance of 3 cm. The optical properties of the inclusions were examined under both static and dynamic temporal states. In the latter case, temporal variability in the absorption coefficient was introduced by assigning values to $\mu_a$ that correspond to different mathematical functions. The specific functions chosen were meant only as representatives of the varying degrees of complexity associated with vascular reactivity that likely exists *in vivo*. The absorption coefficient of the right-hand-side inclusion varied according to a quasiperiodic series, while that of the left-hand-side inclusion varied according to a particular solution of the Hénon equation.[20] A quasiperiodic time course was calculated from the equation $q_n = [\cos(\pi/8)n + \sin(\sqrt{\pi}/4)n]/2$. A Hénon-function time course was calculated from the formula $h_n = (1 + 0.3h_{n-2} - 1.4h_{n-1}^2)/1.3$, with numbers sampled from a random variable uniformly distributed between $-1$ and $+1$ as the two initial values. In each case, the temporal mean value of $\mu_a$ for the inclusions was 0.12 $\text{cm}^{-1}$ and the modulation depth was 20%. The reduced scat-

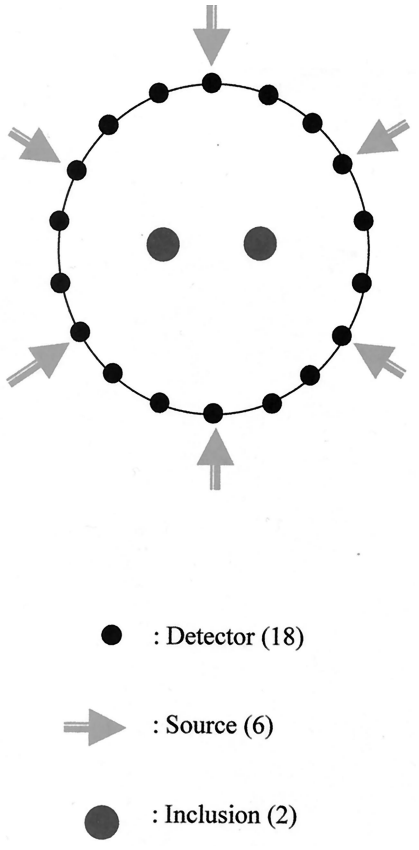


Fig. 1. Geometry and composition of the tissuelike target media and source–detector configuration used for measurement simulations and imaging reconstructions. Target diameter, 8 cm; inclusion diameter, 1 cm; distance between inclusions' centers, 3 cm.

tering coefficient of the inclusions was time invariant and had a value of 15 $cm^{-1}$. The optical properties of the background also were static, with $\mu_a = 0.06$ $cm^{-1}$, $\mu_s' = 10$ $cm^{-1}$. That is, we considered conditions wherein the optical properties of the inclusions differed from those of the background in both coefficients, but temporal variability was limited to only $\mu_a$.

In a second series of studies, we examined the stability of reconstruction results over a broad range of values for the reference medium. In these cases, the optical properties of both the inclusions and the background were static. The structure of the medium was the same as before. The optical properties of the background were similar to the dynamic case, differing only in that the value for $\mu_a$ was 0.04 $cm^{-1}$. The coefficient values for the inclusions were set to $\mu_a = 0.02$ $cm^{-1}$ and $\mu_s' = 5.0$ $cm^{-1}$.

### B. Photon-Propagation Model—Forward Problem

Light propagation in a scattering medium was modeled as a diffusion process. For a domain $\Lambda$ with boundary $\partial\Lambda$, this is represented by the expression

$$\nabla \cdot [D(\mathbf{r})\nabla\phi(\mathbf{r})] - \mu_a(\mathbf{r})\phi(\mathbf{r}) = -\delta(\mathbf{r} - \mathbf{r}_s), \qquad \mathbf{r} \in \Lambda, \tag{5}$$

where $\phi(\mathbf{r})$ is the photon intensity at position $\mathbf{r}$, $\mathbf{r}_s$ is the position of a dc point source, and $D(\mathbf{r})$ and $\mu_a(\mathbf{r})$ are the position-dependent diffusion and absorption coefficients, respectively. Here we use the definition given above (see Section 2) for the diffusion coefficient [and therefore $D(\mathbf{r})$ has dimensions of length rather than, as in the alternative convention adopted by certain other groups, of length squared divided by time[21]], and the $\delta$ in the source term on the right-hand side of Eq. (5) denotes the Dirac delta function. Solutions to the forward problem were obtained by use of a finite-element method that employed a preconditioned conjugate-gradient algorithm[22] for numerically solving the associated systems of linear equations.

### C. Computation of Tomographic Data—Forward Problem

When photon intensity values were computed in the manner just outlined, Dirichlet boundary conditions on an extrapolated boundary were imposed on the solution. Depending on the problem, sources and detectors were positioned 1–2 transport mean-free-path lengths below the extended surface. Source–detector geometry consisted of six sources spaced 60° apart (positions indicated by arrows in Fig. 1), with eighteen detectors per source, also equally spaced about the circumference (positions indicated by small circles in Fig. 1), for a total of 108 source–detector pairs.

Tomographic data sets modeling dynamic behavior were computed, with the above-described illumination conditions, for each of 1000 consecutive time points in the dynamic imaging study and for every combination of reference medium properties considered in the reconstruction stability study.

### D. Image Reconstruction–Inverse Problem

A conjugate gradient descent algorithm was used to reconstruct images by numerically solving Eq. (3).[19] In producing the results presented below, these computations were limited to 1000 iterations within the first-order Born solution.

In the dynamic imaging study, reconstructions were carried out for several specified reference media to produce sets of image time series, which were subjected to further analysis with methods described below. The specific results presented in Section 4 were produced from inverse-problem computations that took only the $\mu_a$ perturbation as the unknown quantity $\delta\mathbf{x}$ in Eq. (3). (We note that qualitatively similar results, not shown, were obtained when $\delta\mathbf{x}$ comprised the perturbations in $\mu_a$ and $D$ simultaneously.) In the reconstruction stability study, tomographic data were analyzed by reconstructing images of $\mu_a$ and $D$ simultaneously under conditions listed in Table 1.

### E. Analysis of Time-Series Image Data

To evaluate the quality of the information obtained from the computed image time series, we generated, using the "method of delays,"[23] pseudo-state-space (PSS) trajectories from the pixel time-series data. This is a standard approach for providing a geomet-

Table 1. Summary of the Test Cases Explored[a]

| Test Case | | Parameters Involved | | | | Range of Reference Optical Properties | | Where Results Are Presented |
|---|---|---|---|---|---|---|---|---|
| No. | Formulation ($\mathbf{W}\delta\mathbf{x} = \delta\mathbf{u}$) | $\mathbf{u}$ | $\mathbf{u}_0$ | $\mathbf{u}_r$ | $\mathbf{W}_r$ | $\mu_a$ (cm$^{-1}$) | $\mu_s'$ (cm$^{-1}$) | |
| 1 | $\mathbf{W} = \mathbf{W}_r$, $(\delta\mathbf{u})_i = \dfrac{u_i - (\mathbf{u}_0)_i}{(\mathbf{u}_0)_i}(\mathbf{u}_r)_i$ | C | C | V | V | 0.0–0.3 | 3–30 | $6 \times 6$ Matrix (Fig. 5) |
| 2 | $\mathbf{W} = \mathbf{W}_r$, $(\delta\mathbf{u})_i = u_i - (\mathbf{u}_r)_i$ | C | — | V | V | 0.02–0.08 | 5–15 | $5 \times 5$ Matrix (Fig. 6) |
| 3 | $\mathbf{W} = \mathbf{W}_r$, $(\delta\mathbf{u})_i = (\mathbf{u}_r)_i \ln\left[\dfrac{u_i}{(\mathbf{u}_r)_i}\right]$ | C | — | V | V | 0.0–0.3 | 3–30 | $6 \times 6$ Matrix (Fig. 7) |
| 4 | $\mathbf{W} = \mathbf{W}_r$, $(\delta\mathbf{u})_i = u_i - (\mathbf{u}_b)_i$ | C | — | C | V | 0.0–0.3 | 3–30 | $6 \times 6$ Matrix (Fig. 8) |
| 5 | $\mathbf{W} = \mathbf{W}_b$, $(\delta\mathbf{u})_i = u_i - (\mathbf{u}_r)_i$ | C | — | V | C | 0.02–0.06 | 5–15 | $5 \times 5$ Matrix (Fig. 9) |

[a]The symbol V designates the parameter that was varied; C, a parameter whose value was held constant. The type of weight matrix used in each simulation study, and the expression for the $i$th source–detector pair of the data vector, are given under Formulation. The symbols $b$ and $r$ designate background and reference, respectively.

rical rendering of a function that can greatly facilitate qualitative inspection of results, as the trajectory that is produced frequently reveals the presence and nature of temporal correlations that are not evident from casual inspection of quantity versus time plots. A time series consisting of numbers $x_1, x_2, \ldots, x_n$ is "embedded" into a PSS of dimension $m$ by sorting of the $x$s into $m$-dimensional vectors $\mathbf{X}_1 = [x_1, x_{1+\tau}, \ldots, x_{1+(m-1)\tau}]$, $\mathbf{X}_2 = [x_2, x_{2+\tau}, \ldots, x_{2+(m-1)\tau}]$, and so on; the parameter $\tau$ that appears here is called the "time delay." Selecting the "correct" values for $m$ and $\tau$ in a given case remains something of an art, although useful guidelines have been given by Griffith,[24] and a lower limit for $m$ can be obtained by the "method of false nearest neighbors."[25] In many cases it is found that the $m$-dimensional vectors eventually are confined to a distinct subset of all the points in the PSS; this subset is then referred to as the "attractor" for the dynamical system that produced the time series.

## 4. Results

### A. Fidelity of Dynamic Measures

Motivating the current study were two anecdotal findings that we had previously noted on a number of occasions: (i) dynamic features can be extracted from the image data with remarkable accuracy, and they can produce maps having high contrast even if the quality of any individual image in the time series is comparatively modest; (ii) the quality of the reconstructed images and the accuracy of the derived dynamics depend only weakly on the choice of the reference medium, a finding that strongly contrasts with the sensitivity that absolute measures have on the accuracy of the initial guess. An example of the dichotomy observed in the first case is shown in Fig. 2. In panels (a)–(c) we show representative reconstructed images obtained at different points in the time series. Recall that we obtained these results by expressing the input data vectors as relative variations about the temporal mean value. In addition, for the purpose of comparison with other results shown below, we assumed prior knowledge of the optical properties of the background. Comparison of these results with the original shown in Fig. 1 reveals that whereas the two-object structure is well revealed, spatial blurring is evident, as is the presence of low-amplitude artifacts in the background. We characterize these as results having modest quality. It is worth emphasizing that we are aware that the image quality can be improved with additional computational effort (e.g., recursive updates). Instead, we have intentionally limited this effort to a first-order solution, to retain reasonable computing times for the time series (1000 images). Nevertheless, as is shown subsequently, we find that even with this constraint the functional form of the inclusions can be extracted from the image series with remarkable accuracy.

Data in panels (a) and (b) of Fig. 3 show plots of the temporal functions assigned to the left- and right-hand inclusions and geometrical renderings of these as PSS attractors. It is apparent that the dynamics of the two inclusions have quite different functional forms. In panels (c) and (d) we show the corresponding plots of the reconstructed time series for selected pixels lying within the boundaries of the recovered inclusions. Comparison reveals that the reconstructed time-series results agree remarkably well with the functional forms of the original. The considerable fidelity of these results stands in sharp contrast to the comparatively lower quality of the reconstructed images from which the dynamic features were derived.

### B. Sensitivity of Dynamic Measures to Systematic Errors

The second characteristic feature we have observed when using Eq. (3) is the relative insensitivity of the reconstruction results and extracted dynamics to er-

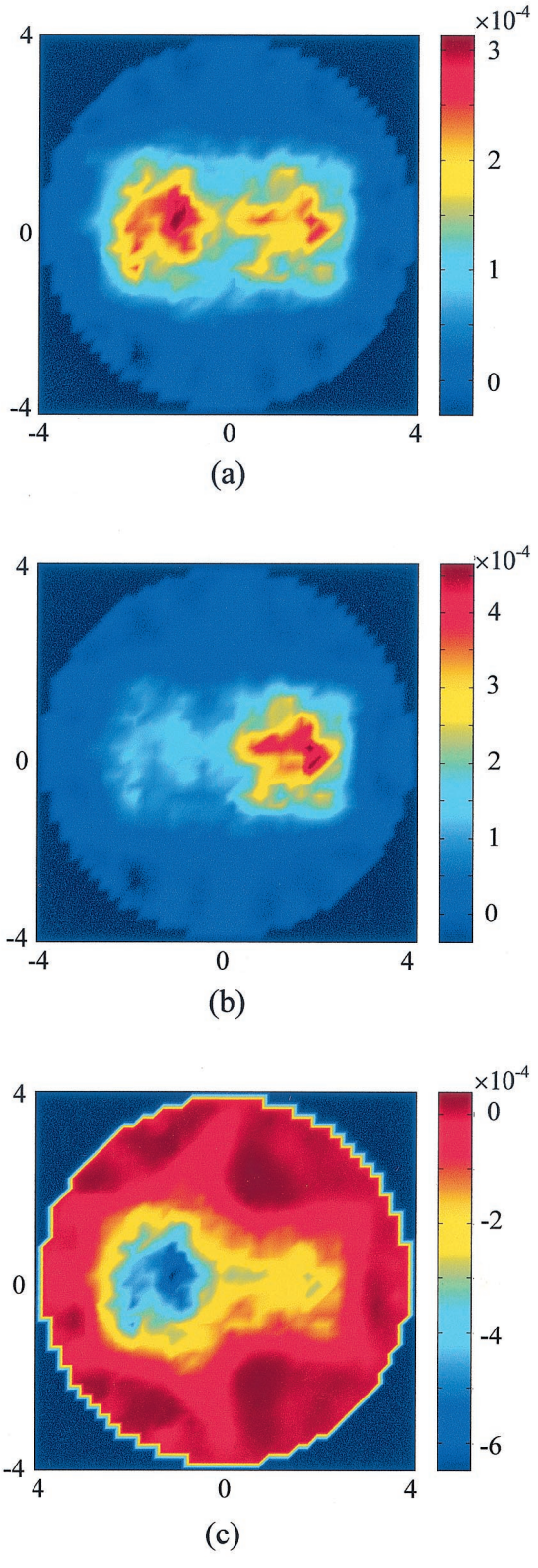


Fig. 2. Reconstructed images of absorption coefficient obtained at time points (a) 1, (b) 5, and (c) 13, based on the simulated dynamic measurement data associated with the time-varying absorption [see Figs. 3(a) and 3(b) for functional form of fluctuations]. Accurate prior knowledge of the optical properties of the background, i.e., $\mu_a = 0.06\ \text{cm}^{-1}$ and $\mu_s' = 10\ \text{cm}^{-1}$, was assumed.

rors in the initial guess (i.e., the reference medium). This is shown by the results in Fig. 4. Panels (a) and (b) show images reconstructed under the conditions modeled in Fig. 3, except that here we used a reference medium whose background absorption and scattering coefficients differed considerably from those of the actual target background. The specific results presented here were obtained with a reference medium having optical properties of $\mu_a = 0.02\ \text{cm}^{-1}$ and $\mu_s' = 25.0\ \text{cm}^{-1}$, which are 0.33 and 2.5 times the true background values, respectively. Comparison of these results with those in Fig. 3 reveals that functional forms of the two are almost identical. We note that similar results were obtained in the case of a reference medium whose properties were $\mu_a = 0.2\ \text{cm}^{-1}$ and $\mu_s' = 3.0\ \text{cm}^{-1}$, as well as for many other cases wherein the absorption and scattering coefficients lay between these extremes. We have also obtained similar findings for dynamic states having wholly different functional forms (e.g., stochastic), including in the limiting case of spatiotemporally coincident dynamic behavior in two different optical parameters (either $\mu_a$ and $\mu_s'$ at a single wavelength[26] or $\mu_a$ at two different wavelengths[7,27]). These findings confirm that the temporal features of dynamic states in dense scattering media can be defined with a high level of accuracy that is largely independent of the selected reference medium used.

In the next several figures we explore this phenomenology in more detail. Of particular interest is to gain a clearer understanding as to *why* analysis of relative measures [Eq. (3)] should produce stable results when, as will be shown, its counterpart [i.e., the standard perturbation formulation, Eq. (1)], is highly unstable to errors stemming from an insufficiently accurate estimate of the reference medium.

### C. Dependence of Image Quality on Accuracy of Reference Medium

Solutions to a perturbation formulation ordinarily require three types of input data. The vector $\mathbf{u}$ (the surface detector responses) is usually obtained from measurements on the target medium, and the other two quantities, $\mathbf{u}_r$ and $\mathbf{W}_r$ (the reference intensity vector and weight functions, respectively), are derived from solutions to the forward problem for a specified reference medium. In the linear approximation, to achieve an accurate reconstruction, the properties of the reference medium should closely approximate those of the target. As this difference grows, so too will the error in the recovered coefficient values. We have explored this dependence by varying the parameters listed in Table 1 and computing solutions according to different formulations of the perturbation equation. The target medium examined was similar to that shown in Fig. 1, having the same geometric structure and physical dimensions but slightly different optical coefficients. In this case the background optical properties were $\mu_a = 0.04\ \text{cm}^{-1}$ and $\mu_s' = 10\ \text{cm}^{-1}$, while in the inclusions both coefficients were halved. For each case examined we explored the dependence of the quality of the

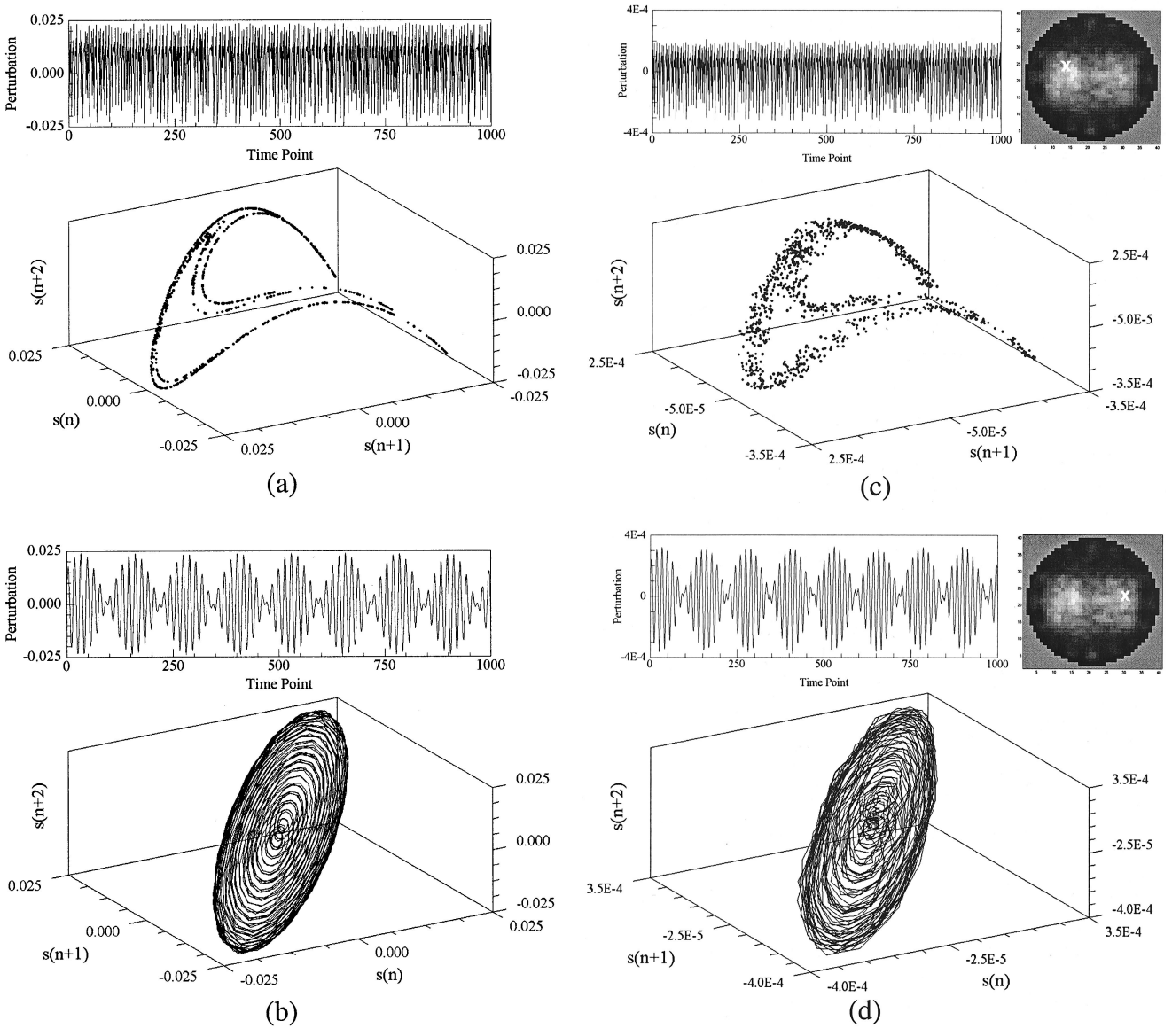


Fig. 3. Panels (a) and (b) are plots of the temporally fluctuating $\mu_a$ assigned to the left- and the right-hand inclusions, respectively, and the corresponding PSS trajectories for $m = 3$, $\tau = 1$ (see Subsection 3.E for explanation of symbols). Panels (c) and (d) are the corresponding plots of reconstructed time series for selected pixels lying within the two inclusions (examples of individual reconstructed images in the time series are shown in Fig. 2).

reconstructed image on a specified reference medium whose optical properties were varied over selected ranges. In some cases we assumed prior knowledge of the most accurate estimate available for either $\mathbf{u}_r$ or $\mathbf{W}_r$, (i.e., the detector readings and weight functions for a reference medium whose optical properties are identical to those of the background of the target medium) and substituted values for the remaining input data that were computed for a different (i.e., inaccurate) selected reference medium. Test cases 1–3 explored the general case in which no specific knowledge of the test medium is available. The ranges of optical properties examined for the reference medium were 0.0–0.3 $\text{cm}^{-1}$ for $\mu_a$ and 3–30 $\text{cm}^{-1}$ for $\mu_s'$ in cases 1 and 3, and 0.02–0.08 $\text{cm}^{-1}$ for $\mu_a$ and 5–15 $\text{cm}^{-1}$ for $\mu_s'$ in case 2. As will be shown, compared with the standard perturbation formulation using either the Born or the Rytov approximation, significantly improved image quality is achieved by use of the NDM formulation. Test cases 4 and 5 assumed prior knowledge of the optical properties of the background medium from which either $\mathbf{u}_r$ or $\mathbf{W}_r$ is computed, and they substitute values that correspond to different reference media for the remaining input data.

Images were reconstructed as before, with the above-mentioned conditions for data collection, with the exception that both coefficients $\delta\mu_a$ and $\delta D$, represented as $\delta\mathbf{x}$ in Table 1, were reconstructed simultaneously.

Data in Fig. 5 show the reconstruction quality obtained as a function of the optical properties of the

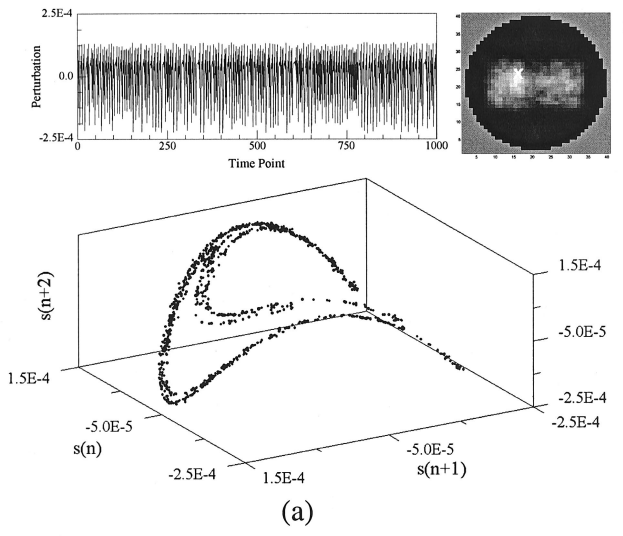


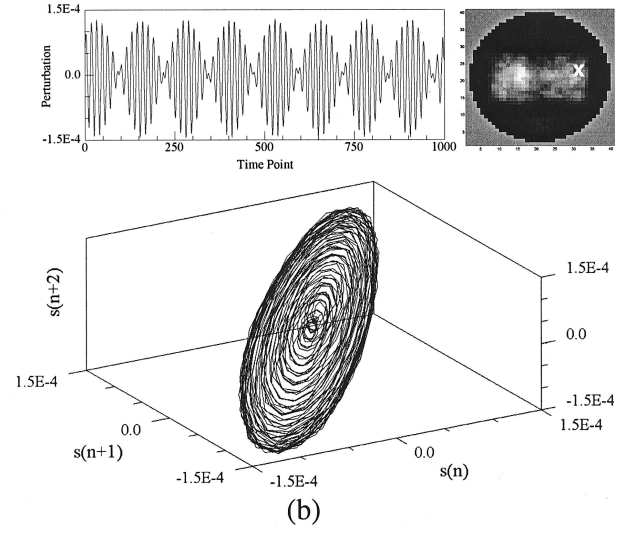


Fig. 4. Demonstration of weak dependence on reference medium properties of image time series obtained by use of Eq. (3) to perform the reconstructions. Conditions modeled are the same as for Fig. 3, except that optical coefficients of reference medium are $\mu_a = 0.02\ \mathrm{cm}^{-1}$ and $\mu_s' = 25\ \mathrm{cm}^{-1}$. Panels (a) and (b) are time courses and corresponding PSS trajectories for selected pixels in the left- and the right-hand inclusions, respectively.

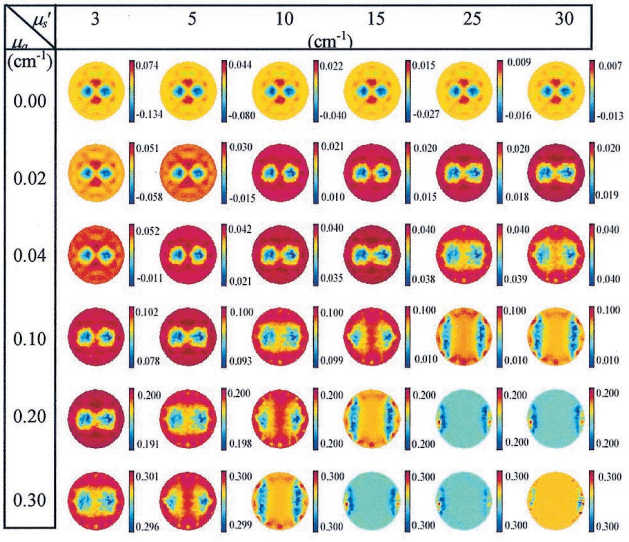


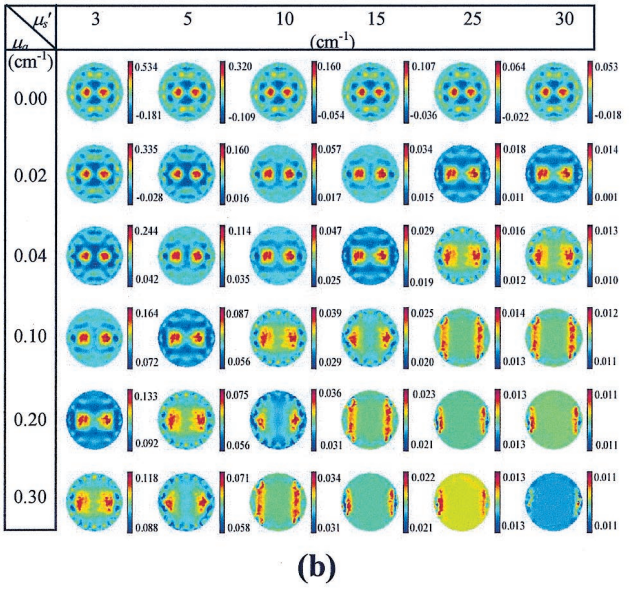


Fig. 5. Results obtained from test case 1 listed in Table 1 {i.e., NDM formulation [Eq. (3)], "experimental" data fixed, reference medium properties are varied}: (a) absorption profiles, (b) diffusion profiles.

reference medium. Panel (a) shows the computed absorption maps; panel (b), the computed diffusion maps. Recall that the true background properties are $\mu_a = 0.04\ \mathrm{cm}^{-1}$ and $\mu_s' = 10.0\ \mathrm{cm}^{-1}$. Inspection reveals that the two-object structure is recovered for both coefficients over nearly the entire matrix, with the exception of cases in which both the absorption and scattering coefficients of the reference medium are significantly greater than those of the true background. Note that these results were obtained with the NDM formulation, which requires consideration of two different experimental measures. In the previous examples (Figs. 2–4), one quantity was the detector reading at a specific time point and the other was the corresponding temporal mean value. As indicated, other forms of relative measures can be considered as well. In the present case, we consider data obtained in the presence and the absence of the inclusions. A practical example of this could be data obtained before and after administration of a dye. These data are examined in a more quantitative manner below.

Shown in Fig. 6 are the results corresponding to those in Fig. 5 but obtained when the standard perturbation formulation [Eq. (1)], in a first-order Born

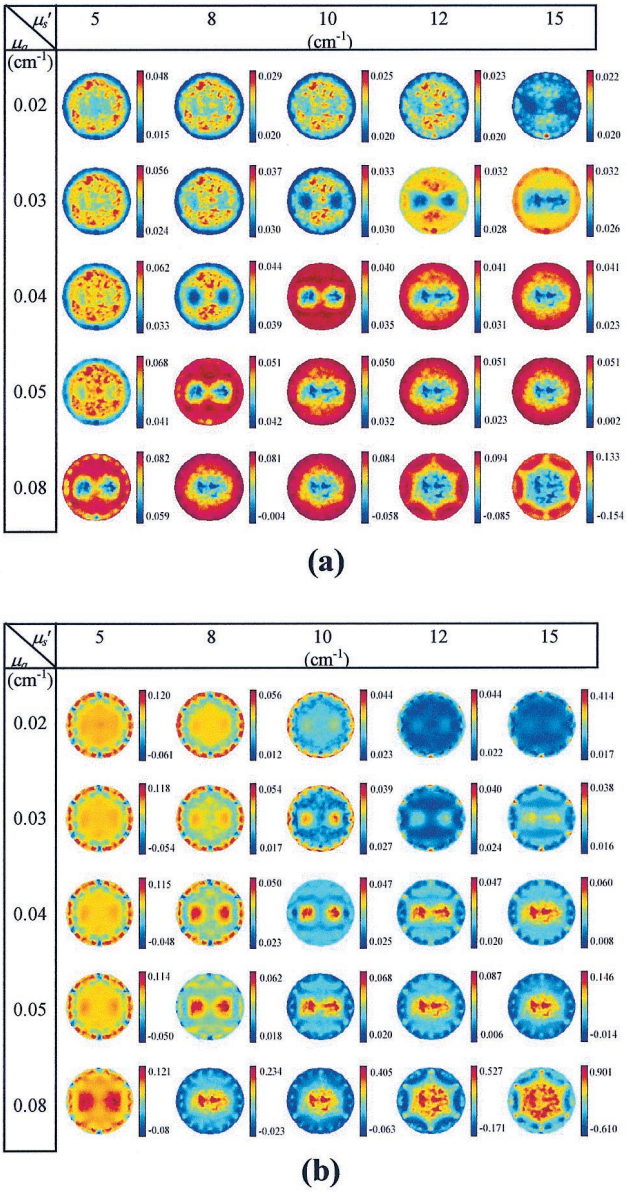


Fig. 6. Results obtained from test case 2 listed in Table 1 {i.e., conventional first-order Born formulation [Eq. (1)], "experimental" data fixed, reference medium properties are varied}: (a) absorption profiles, (b) diffusion profiles. Note that in every instance, the set of reference properties used in the calculation of the computed detector readings is the same as that used in the calculation of the imaging operator.

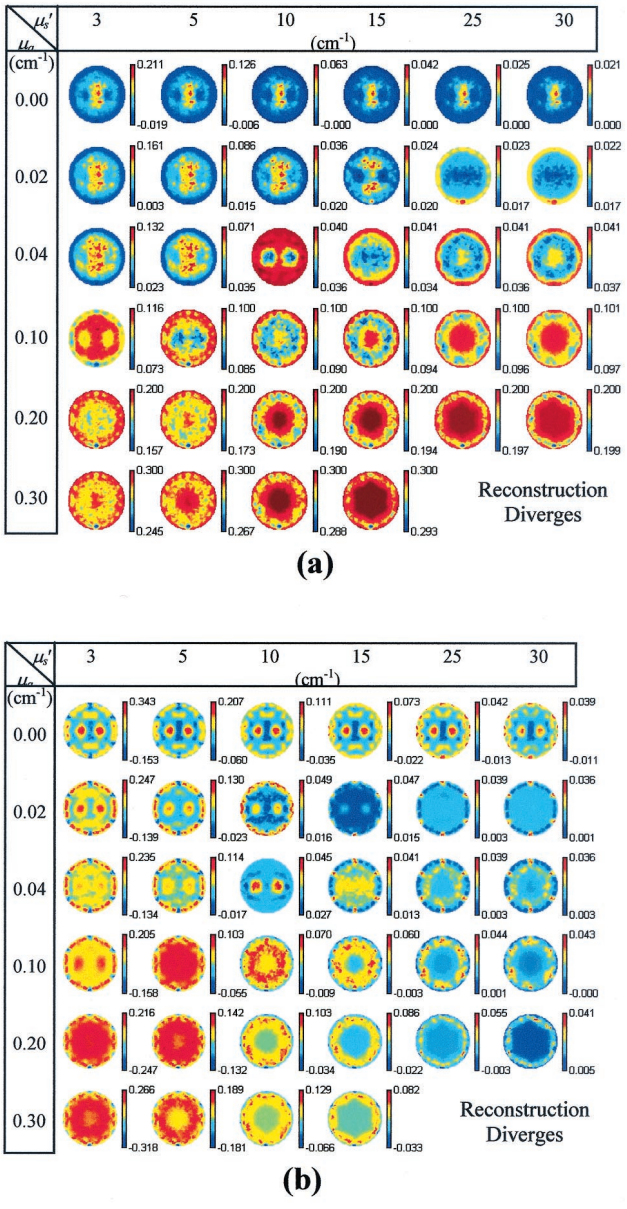


Fig. 7. Results obtained from test case 3 listed in Table 1 (i.e., conventional first-order Rytov formulation, "experimental" data fixed, reference medium properties are varied): (a) absorption profiles, (b) diffusion profiles. Note that in every instance, the set of reference properties used in the calculation of the computed detector readings is the same as that used in the calculation of the imaging operator.

approximation, was used instead of Eq. (3). Note that the ranges of absorption and scattering coefficients considered for the reference medium are considerably smaller in Fig. 6 than in Fig. 5. Inspection reveals that the two-object structure is revealed within a much more restricted range, outside of which only artifact is recovered. Results of a similar analysis that employed the Rytov approximation are shown in Fig. 7. In this case we see some evidence of an improved solution over a range greater than that provided for by the Born approximation but still small compared with the range over which qualitatively accurate reconstructions are achieved using the NDM algorithm. It is clear that the stability of the two formulations [i.e., Eq. (1) versus Eq. (3)] to insufficiently accurate knowledge of the reference medium is quite different. To gain insight as to why this should be, we have considered two other cases, in which we assumed accurate prior knowledge of either the reference detector readings *or* the weight matrix values.

Data in Fig. 8 show the results obtained with the most accurate knowledge of the reference detector readings $\mathbf{u}_r$ available (i.e., those corresponding to a

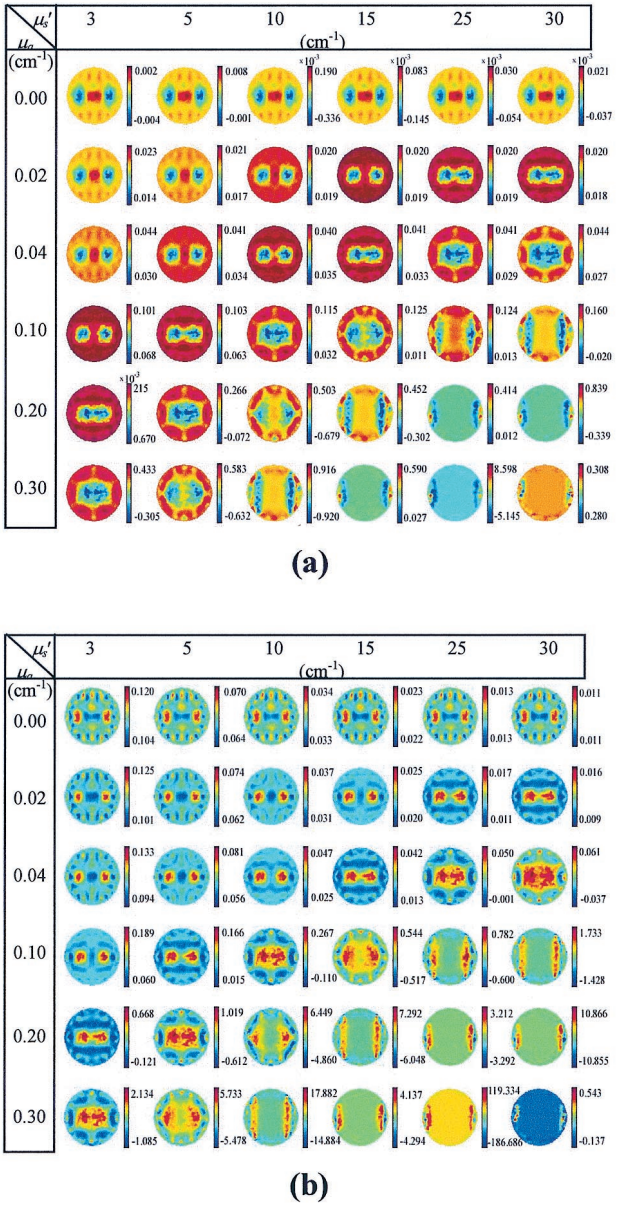


Fig. 8. Results obtained from test case 4 listed in Table 1 {i.e., conventional first-order Born formulation [Eq. (1)], "experimental" data and computed detector readings fixed, reference medium properties used for computation of imaging operator are varied}: (a) absorption profiles; (b) diffusion profiles.

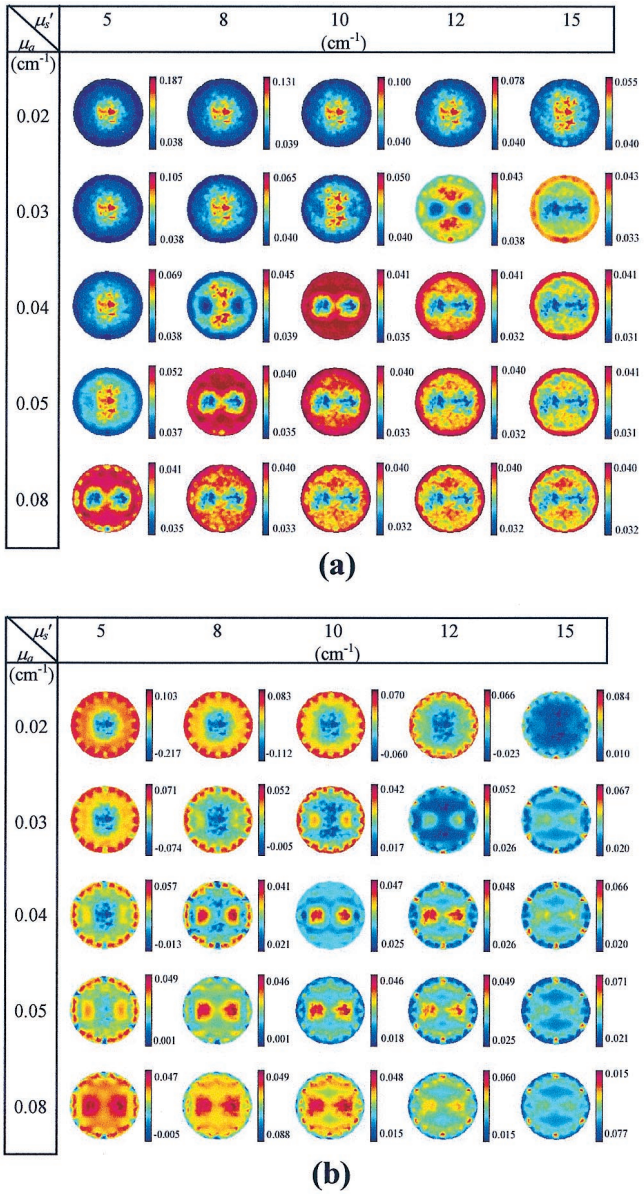


Fig. 9. Results obtained from test case 5 listed in Table 1 {i.e., conventional first-order Born formulation [Eq. (1)], "experimental" data and imaging operator fixed, reference medium properties used for computation of computed detector readings are varied}: (a) absorption profiles; (b) diffusion profiles.

homogeneous medium whose optical coefficients are identical to those of the background of the target medium). In this case, only the values of the weight functions are varied; the substituted $\mathbf{W}_r.s$ were computed from reference media whose absorption and scattering coefficients lay in the ranges indicated in row 4 of Table 1. Inspection of these results shows that, qualitatively, they are nearly identical to those in Fig. 5 (quantitative differences are present). Significantly, these results and those shown in Fig. 6 were both obtained with the standard perturbation formulation. The only difference is in the accuracy with which the reference detector readings are known. For results shown in Fig. 8, the $\mathbf{u}_r.$ used was maximally accurate, while for those shown in Fig. 6, in most cases it was not. This suggests that the principal cause of instability is insufficiently accurate knowledge of $\mathbf{u}_r.$.

This possibility is directly explored by the study whose results are shown in Fig. 9. Here we considered a situation similar to that adopted for Fig. 8 except that the most accurate knowledge of $\mathbf{W}_r.$, rather than $\mathbf{u}_r.$, is available. Recall that this is the case in which properties of the reference medium equal the background properties of the target medium. While $\mathbf{W}_r.$ was thus fixed, $\mathbf{u}_r.$ values were computed from reference media whose optical coefficient values varied over the ranges indicated in row 5 of

Table 1. Similar to results shown in Fig. 6, the results obtained indicate that the two-object structure is revealed over only a limited range of reference medium absorption and scattering coefficients. These findings confirm that the excessive sensitivity of the standard perturbation formulation to an insufficiently accurate estimate of the reference medium is primarily a consequence of errors in the estimated intensity values and not of corresponding errors in the imaging operators. This is a new finding, and as discussed below, one we believe holds considerable significance for practical imaging studies.

## 5. Discussion

### A. Analysis of Different Sensitivities of Standard Perturbation and NDM Methods

In this paper we have examined the reliability of information obtained from optical tomographic image data generated with linear perturbation methods. The accuracy of recovered images of perturbations in the absolute coefficient values, maps revealing relative changes in these quantities, and information regarding the dynamic state of inclusions all were examined. Results obtained demonstrate that when limited to a first-order solution, the accuracy of the derived information depends strongly on the optical properties of the selected reference medium. The sensitivity of these measures to an insufficiently accurate reference obeys the following inequality: Absolute coefficient values $\gg$ relative change in coefficient values $>$ dynamic state of coefficient values. Given the expected range of uncertainties associated with tissue measurements, it seems doubtful that estimates of the properties of an appropriate reference medium can be obtained with sufficient accuracy to avoid artifact-dominated results, at least when restricted to first-order solutions. While this situation may improve with additional computational effort, it seems likely that the improvement will be accompanied by a diminishing rate of return. We wish to emphasize that the indicated inequality holds irrespective of whether the Born or the Rytov approximation for Eq. (3) was evaluated. Further, as noted in the text, whereas we confirmed previously reported differences in the sensitivity between the two approximations for the standard perturbation scheme [Eq. (1)],[5] these differences were largely minimized when Eq. (3) was evaluated.

In clinical medicine, as well as with a range of physiological studies, experience has shown that in many instances measures revealing relative changes in a parameter can provide highly useful information. Measures of this type are often employed when one monitors the response to a physiological or a metabolic provocation. In addition, in these cases, the information sought after not infrequently is some type of time-dependent response. In recognition of this we have recently developed experimental systems that are well suited for monitoring time-dependent features of large tissue structures, in a cross-sectional imaging modality operating at near-infrared wavelengths.[8] As a starting point we have sought to evaluate the time-dependent tomographic detector data as relative fluctuations about the temporal mean value. The approach we used was to evaluate the derived data according to Eq. (3). Our experience with this formulation has been that, unlike the strong sensitivity to the reference medium properties observed with the standard perturbation equation [Eq. (1)], the relative contrast of inclusions throughout the reconstructed image is weakly dependent on the choice of the reference medium. It is instructive to understand why the difference between the sensitivities of the two approaches should be so large.

In the case of the standard formulation [i.e., Eq. (1)] the input data vector is actually the difference between a measured and a computed quantity. This vector contains information regarding the subsurface coefficients that, as shown, can be extracted provided that an accurate reference medium is available. The difficulty, however, is that the reference intensity values are extremely dependent on the optical coefficient values of the reference medium. Significantly, this dependence is a nonlinear function of the distance between source and detector. It follows that a small change in the optical properties of the reference medium may significantly influence the value of the computed intensity differences ($\delta\mathbf{u}$) by a relative amount that is different for each source–detector pair, thereby altering the information content of the data vectors. An example of this is shown in Fig. 10.

Figure 10(a) shows the central angle (which is proportional to the source–detector separation) dependence of the computed $\delta\mathbf{u}$, for a source located on the target diameter perpendicular to the line joining the centers of the two inclusions (i.e., the "12 o'clock" position in Fig. 1), for several reference media whose properties correspond to row 3 of Fig. 5. Inspection of the plots clearly reveals a bimodal attenuation profile indicating the presence of two buried objects. In contrast, this structure is almost completely absent from results, shown in Fig. 10(b), derived with the standard perturbation formulation under the same measurement conditions, even though the range of variation of the reference medium is much less than that used to generate the data in Fig. 10(a). This directly demonstrates that the information content of the data vector can be grossly distorted when Eq. (1) is used to evaluate detector data, whereas this information is mainly preserved when Eq. (2) or Eq. (3) is used. This is a critical distinction. It is important to recognize that essentially all tomographic methods effectively are mapping procedures. That is, they project information onto the image domain in accordance with the structure of the operators. In the case of scattering media, the characteristic structure of the weight functions is observed over a wide range of coefficient values. Thus it would seem reasonable to expect that, provided the information content of the data vectors is not corrupted, the use of operators that basically have the correct structure

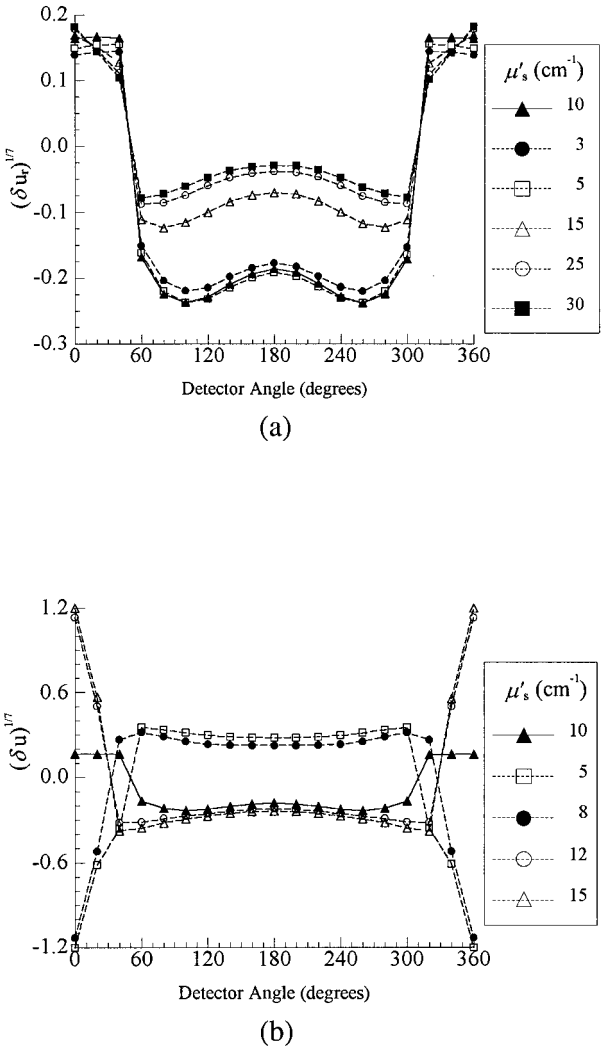


Fig. 10. (a) Dependence of $\delta u_r$, i.e., $(\delta \mathbf{u}_r)_i = (\mathbf{u}_r)_i\{[u_i - (\mathbf{u}_0)_i]/(\mathbf{u}_0)_i\}$, on angular separation between source and detector, for reference-medium properties corresponding to row 3 of Fig. 5 (test case 1, NDM formulation). (b) Dependence of $\delta u$, i.e., $(\delta \mathbf{u})_i = u_i - (\mathbf{u}_r)_i$, on angular separation between source and detector, for reference-medium properties corresponding to row 3 of Fig. 6 (test case 2, standard Born formulation). The source located at the "12 o'clock" position indicated in Fig. 1 was used for both panels. Because the quantities plotted on the ordinate scales take on positive and negative values, logarithmic scaling is not appropriate. Instead, we make use of the transformation $y = x^{1/n}$, with $n = 7$ in the examples plotted here, to permit the display of data ranging over several orders of magnitude on a single set of axes.

should result in recovery of images that are at least qualitatively correct. It is our belief that this explains the results shown in Figs. 3 and 4. These data also confirm and extend results reported by Graber *et al.*, who observed a similar phenomenon when reconstructing images while using weight functions derived from numerical (Monte Carlo simulations) solutions of the transport equation.[28]

It is important to recognize that the sensitivity of the reference medium's detector readings to small variations in its optical coefficients is inherent in the physics of light propagation in scattering media and so would persist even if the measurement data were error free. Thus, whereas much effort has been devoted to improving the computational efficiency of the standard perturbation scheme[29] and its stability to noise,[19] it seems that these efforts may have limited practical value when applied to imaging studies of tissue, in view of the expected difficulties associated with identifying a sufficiently accurate reference medium.

### B. Stability of Dynamic Measures

Motivating our interest in the use of dynamic imaging methods is the fact that the time dependence of a measured or derived property, especially if it is associated with a complex system, frequently exhibits meaningful phenomenology that is simply undetectable from static observations. Importantly, in many cases useful quantitative descriptions of these are independent of the amplitude of a measured response. For instance, the temporal cross-correlation function[30] of a data time series and the frequency structure[31] of its Fourier transform are independent of the amplitude of the signal. Parameters of interest in the study of nonlinear chaotic systems, such as the shape of an attractor, its correlation dimension,[32] and its Lyapunov exponent spectrum,[20] also are insensitive to signal amplitude.

An observation we have made, which may be of considerable practical value and which is related to the foregoing discussion on sensitivity to choice of reference medium, concerns the stability of dynamic measures. In our dynamic imaging efforts, one consistent finding has been that the quality of derived dynamic measures is considerably more accurate, both qualitatively and quantitatively, than that of the image time series from which they were extracted. The reason, more fully developed elsewhere,[33] why this observation is not surprising is that while the specific numerical values of the reconstructed coefficients are not quantitatively accurate, in each pixel the relative error is highly consistent throughout the image time series. The only necessary condition for quantitatively accurate determination of the above-mentioned dynamic properties, and others[33] is that, over time, the reconstructed coefficient be nearly a linear function of the true coefficient value. Each pixel is independent of the others for this purpose; i.e., the numerical values of the parameters in these linear relations can be different in every one. The key issue then becomes the following: Under what circumstances is it most probable that the relations between true and reconstructed optical coefficients will in fact be linear? The results and preceding discussion indicate that this is best accomplished with a reconstruction method based upon relative differences between detector readings, because of its reduced sensitivity to the difference between the properties of the target and reference media.

Another issue related to dynamic investigations concerns the potential diagnostic sensitivity and specificity of dynamic measures compared with that of information obtained directly from images of rela-

Table 2. Ratio of Average Contrasts of Reconstructed Absorption and Diffusion Coefficients Shown in Figs. 5(a) and 5(b), Respectively[a,b]

| $\mu_a$ (cm$^{-1}$) \ $\mu_s'$ (cm$^{-1}$) | 3 | 5 | 10 | 15 | 25 | 30 |
|---|---|---|---|---|---|---|
| 0.00 | 0.3427 | 0.3435 | 0.3441 | 0.3429 | 0.3427 | 0.3429 |
| 0.02 | 0.3627 | 0.3682 | 0.3882 | 0.4000 | 0.3846 | 0.3469 |
| 0.04 | 0.3715 | 0.3887 | 0.4042 | 0.3608 | 0.2758 | 0.2380 |
| 0.10 | 0.4048 | 0.3817 | 0.2816 | 0.1891 | 0.2000 | 0.0000 |
| 0.20 | 0.3463 | 0.2761 | 0.1212 | 0.1428 | 0.0000 | 0.0000 |
| 0.30 | 0.2863 | 0.1683 | 0.1000 | 0.0000 | −NAN[c] | −NAN |

[a]Matrix format is the same as that of Fig. 5 [for the target medium, $\delta\mu_a/\delta D = 0.02/0.0332 = 0.6024$, $(\delta\mu_a/\delta D)^2 = 0.3626$].

[b]To minimize the effect of near-surface artifacts on these computed ratios, $\delta\mu_a$ and $\delta D$ were averaged over only the area lying within 2 cm (i.e., half the radius of the target medium) of the center of each image.

[c]NAN means "not a number" and here indicates that the quantity $\delta D$ was equal to zero throughout the entire area included in the computation of $\delta\mu_a/\delta D$.

tive optical contrast. To be clear, we recognize that whereas the former is derived from a time series of the latter, the two are not equivalent in terms of the feasibility of meaningfully comparing data obtained for different individuals within a population. This issue here is not one of biology but is a practical matter associated with the analysis schemes used. Assume for the moment that measurement of some relative change in optical coefficient value (for instance, in response to a specific provocation) has the same intrinsic diagnostic value as does a measured or a derived dynamic response. As we have shown here, the latter type of information (e.g., functional form of the dynamic process) is essentially independent of the chosen reference medium.[34] However, whereas this information comes from our analysis of relative measures, the choice of the reference medium certainly does influence the amplitude of the relative response itself. Given the variability of tissue size and composition, it is likely that comparison of measures among individuals will require selection of some range of reference values, which would result in relative measures having a higher variance than a corresponding dynamic measure.

### C. Quantitative Analysis of Image Data Provided by the NDM Algorithm

As one might expect, use of reference media that increasingly differ from the true target background will produce results having correspondingly greater errors in the estimated unknown coefficients. While this is seen (cf. Fig. 5), we have nevertheless observed some interesting quantitative dependencies that may have practical value. One such finding is that whereas the computed coefficient values $\delta\mu_a$ and $\delta D$ depend strongly on the reference medium properties, the ratio $\delta\mu_a/\delta D$ is nearly independent of them. This result is seen in Table 2 for image data presented in Fig. 5. In fact, for the examples studied, we find that $(\delta\mu_a/\delta D)_{\text{Image}} \approx (\delta\mu_a/\delta D)^2_{\text{Target}}$ over most of the range of reference values explored. In other examples (results not shown) we have explored this relationship for a variety of perturbation values for the inclusions, with a similar range of reference media. In all cases a constant error in the ratio of the derived coefficients was obtained. The value of the proportionality constant, however, varied depending on the magnitude and direction of the perturbation but remained within a relatively small range. Interestingly, this coefficient ratio is closely related to a quantity known as the *diffusion length* ($L$), which is related to the more familiar properties by $L = (D/\mu_a)^{1/2}$. Thus, if it can be shown that the observed relationship is a general feature of images reconstructed under the NDM formulation, it would suggest that perturbations in $L$ can be recovered with greater accuracy than can either the absorption or the diffusion coefficient.

Another observation we have made is that use of reference media whose coefficient values are smaller than those of the true background in many cases results in reconstructions wherein the optical coefficient values are significantly overestimated but which are relatively free of artifact. We mention this because it may represent a simple numerical means whereby the contrast of the inclusions can be enhanced.

### D. Comparison with Other Recent Studies

An earlier study of the quantitative effect on reconstructed images of differences between the background optical coefficients of the target medium and those assigned to the reference medium was published by Cheng and Boas.[35] Consistent with the results presented here, they report that underestimating or overestimating the background absorption or scattering coefficient by even a small amount produces large errors in the numerical values of the reconstructed coefficients (they do not address spatial resolution or other qualitative aspects of reconstruction accuracy). It also is demonstrated that the *ratio* of two reconstructed coefficients has a quantitative error that is many times smaller than the error in each by itself. While this does not provide a complete analogy to the studies reported on here, because they did not evaluate relative changes in detector readings, their findings are nonetheless consistent with our observations. We find additional grounds for optimism that the NDM formulation will have general utility in the fact that the principal features of the results that Cheng and Boas present do not depend on the choice of image-reconstruction algorithm and that their images were reconstructed from data obtained in a limited-view measurement (reflectance from a single surface, or transmission through a slab). It would thus appear that the advantages of the NDM formulation are independent of choice of measurement geometry (i.e., it has been directly demonstrated here for data recorded in the full tomographic mode and is implied by the findings reported in Ref. 35 for the reflectance and transmission modes).

Interestingly, the NDM formulation described here is quite similar to a more general expression derived by Ntziachristos *et al.*,[36,37] who also considered a differential measure. These authors recognized that the generation of interesting contrast features in tissue, such as produced by injection of a dye, or response to a particular provocation, can sufficiently change the average tissue optical properties to limit the accuracy of images recovered on the basis of linear perturbation theory. The expression they derived [Eq. (20) in Ref. 36] effectively removes this average shift, which, in their test example, had the effect of producing images with reduced surface artifacts. Seemingly, the advantage of this scheme is that it allows for evaluation of an expression more in line with the basic premise of perturbation theory (i.e., perturbations are weak). We have found, however, that this improved result is not without its trade-offs. Specifically we have determined (results not shown) that to achieve accurate reconstructions, the ratio of computed intensities [i.e., $U_0'/U_0''$, listed in the left-hand side of Eq. (20)] corresponding to those obtained from the initial guesses of the estimated background optical properties before ($U_0'$) and after ($U_0''$) a provocation, must be known with considerable accuracy. Whereas in practice this might be possible from analysis of time-resolved or equivalent measurement data, we consider it unlikely that similar quality estimates could be derived in the case of dc data. In its absence we have found that reconstruction results derived with their[36] Eq. (20) exhibit a dependence on the accuracy of the initial guess at least as sensitive as do the standard Born and Rytov approximations described here [cf. Eq. (1)].

It is worth pointing out that in the limit where the computed ratio of $U_0'/U_0''$ approaches unity, Eq. (20) of Ref. 36 becomes essentially equivalent to our NDM formulation in the Rytov approximation. Interestingly, the latter expression is exactly equivalent to their Eq. (22), which they refer to as the typical Rytov approximation.[36] We should point out, however, that this description is not in keeping with the "typical Rytov approximation" referred to in the computed tomography literature.[38] The data vector corresponding to the latter, using the notation of Ref. 36, is the quantity $\ln(U'/U_0)$, whereas for the former it is $\ln(U''/U')$, where $U_0$, $U'$, and $U''$ are the detector readings computed for the initial state, measured prior to a provocation and measured following a provocation, respectively. As we have shown here, this distinction is critical. To reiterate, results in Fig. 7 demonstrated that the "typical Rytov approximation" [i.e., $\ln(U'/U_0)$], is quite unstable to insufficiently accurate estimates of the initial guess. In contrast, when evaluated with the NDM scheme, such sensitivity is markedly reduced. Thus it would appear that while the basic benefits of adopting differential schemes are well appreciated,[35–37] what has not been evident until now is how such measures can be evaluated to maximize solution stability.

This research was supported in part by National Institutes of Health (NIH) grant RO1-CA66184.

### References and Notes


1. H. L. Graber, J. Chang, R. Aronson, and R. L. Barbour, "A perturbation model for imaging in dense scattering media: derivation and evaluation of imaging operators," in *Medical Optical Tomography: Functional Imaging and Monitoring*, G. Müller, B. Chance, R. Alfano, S. Arridge, J. Beuthan, E. Gratton, M. Kaschke, B. Masters, S. Svanberg, and P. van der Zee, eds., Vol. IS11 of SPIE Institute for Advanced Optical Technologies Series (SPIE Optical Engineering Press, Bellingham, Wash., 1993), pp. 121–143.
2. R. L. Barbour, H. L. Graber, Y. Wang, J.-H. Chang, and R. Aronson, "A perturbation approach for optical diffusion tomography using continuous-wave and time-resolved data," in *Medical Optical Tomography: Functional Imaging and Monitoring*, G. Müller, B. Chance, R. Alfano, S. Arridge, J. Beuthan, E. Gratton, M. Kaschke, B. Masters, S. Svanberg, and P. van der Zee, eds., Vol. IS11 of SPIE Institute for Advanced Optical Technologies Series (SPIE Optical Engineering Press, Bellingham, Wash., 1993), pp. 87–120.
3. S. R. Arridge, "The forward and inverse problems in time resolved infra-red imaging," in *Medical Optical Tomography: Functional Imaging and Monitoring*, G. Müller, B. Chance, R. Alfano, S. Arridge, J. Beuthan, E. Gratton, M. Kaschke, B. Masters, S. Svanberg, and P. van der Zee, eds., Vol. IS11 of SPIE Institute for Advanced Optical Technologies Series (SPIE Optical Engineering Press, Bellingham, Wash., 1993), pp. 35–64.
4. R. L. Barbour, H. L. Graber, J. Chang, S.-L. S. Barbour, P. C. Koo, and R. Aronson, "MRI-guided optical tomography: prospects and computation for a new imaging method," IEEE Comput. Sci. Eng. **2**(4), 63–77 (1995).
5. M. A. O'Leary, D. A. Boas, B. Chance, and A. G. Yodh, "Simultaneous scattering and absorption images of heterogeneous media using diffusive waves within the Rytov approximation," in *Optical Tomography, Photon Migration, and Spectroscopy of Tissue and Model Media: Theory, Human Studies, and Instrumentation*, B. Chance and R. R. Alfano, eds., Proc. SPIE **2839,** 320–327 (1995).
6. R. L. Barbour, H. L. Graber, C. H. Schmitz, Y. Pei, S. Zhong, S.-L. S. Barbour, S. Blattman, and T. Panetta, "Spatiotemporal imaging of vascular reactivity by optical tomography," in *Proceedings of Inter-Institute Workshop on* in vivo *Optical Imaging at the NIH, 1999* (Optical Society of America, Washington, D.C., 2000), pp. 161–166.
7. H. L. Graber, C. H. Schmitz, Y. Pei, S. Zhong, S.-L. S. Barbour, S. Blattman, T. Panetta, and R. L. Barbour, "Spatio-temporal imaging of vascular reactivity," in *Physiology and Function from Multidimensional Imaging*, A. V. Clough and C.-T. Chen, eds., Proc. SPIE **3978,** 32–43 (2000).
8. C. H. Schmitz, H. L. Graber, H. Luo, I. Arif, J. Hira, Y. Pei, A. Bluestone, S. Zhong, R. Andronica, I. Soller, N. Ramirez, S.-L. S. Barbour, and R. L. Barbour, "Instrumentation and calibration protocol for imaging dynamic features in dense-scattering media by optical tomography," Appl. Opt. **39,** 6466–6486 (2000).
9. S. Sunberg and M. Castrén, "Drug- and temperature-induced changes in peripheral circulation measured by laser-Doppler flowmetry and digital-pulse plethysmography," Scand. J. Clin. Lab. Invest. **46,** 359–365 (1989).
10. S. W. Porges and R. E. Bohrer, "The analysis of periodic processes in psychophysiological research," in *Principles of Psychophysiology: Physical, Social, and Inferential Elements* (Cambridge University, New York, 1991), pp. 708–753.
11. J. Theiler and P. E. Rapp, "Re-examination of the evidence for

low-dimensional, nonlinear structure in the human electroencephalogram," Electroencephalogr. Clin. Neurophysiol. **98,** 213–222 (1996).
12. R. L. Barbour, R. Andronica, Q. Sha, H. L. Graber, and I. Soller, "Development and evaluation of the IRIS-OPTIscanner, a general purpose optical tomographic imaging system," in *Advances in Optical Imaging and Photon Migration*, J. G. Fujimoto and M. S. Patterson, eds., Vol. 21 of OSA Trends in Optics and Photonics Series (Optical Society of America, Washington, D.C., 1998), pp. 251–255.
13. C. H. Schmitz, H. L. Graber, and R. L. Barbour, "A fast versatile instrument for dynamic optical tomography," in *Biomedical Topical Meetings*, Postconference Digest, Vol. 38 of OSA Trends in Optics and Photonics Series (Optical Society of America, Washington, D.C., 2000), pp. 94–96.
14. S. Blattman, H. L. Graber, S. Zheng, Y. Pei, J. Hira, I. Arif, and R. L. Barbour, "Imaging of tissue reperfusion by dynamic optical tomography," in *Biomedical Topical Meetings*, Postconference Digest, Vol. 38 of OSA Trends in Optics and Photonics Series (Optical Society of America, Washington, D.C., 2000), pp. 409–410.
15. S. Blattman, H. L. Graber, S. Zheng, Y. Pei, J. Hira, I. Arif, and R. L. Barbour, "Imaging of differential reactivity of the vascular tree in the human forearm by optical tomography," in *Biomedical Topical Meetings*, Postconference Digest, Vol. 38 of OSA Trends in Optics and Photonics Series (Optical Society of America, Washington, D.C., 2000), pp. 430–432.
16. H. L. Graber, S. Zheng, Y. Pei, I. Arif, J. Hira, and R. L. Barbour, "Dynamic imaging of muscle activity by optical tomography," in *Biomedical Topical Meetings*, Postconference Digest, Vol. 38 of OSA Trends in Optics and Photonics Series (Optical Society of America, Washington, D.C., 2000), pp. 407–408.
17. R. L. Barbour, H. L. Graber, S. Zheng, Y. Pei, J. Hira, and I. Arif, "Optical imaging of the response of vascular dynamics to a cold shock," in *Biomedical Topical Meetings*, Postconference Digest, Vol. 38 of OSA Trends in Optics and Photonics Series (Optical Society of America, Washington, D.C., 2000), pp. 458–460.
18. P. C. Hansen, *Rank-Deficient and Discrete Ill-Posed Problems* (Society for Industrial and Applied Mathematics, Philadelphia, Pa., 1998).
19. Y. Pei, "Optical tomographic imaging using finite element method," Ph.D. dissertation (Polytechnic University, Brooklyn, N.Y., 1999).
20. K. Briggs, "An improved method for estimating Liapunov exponents of chaotic time series," Phys. Lett. A **151,** 27–32 (1990).
21. D. A. Boas, M. A. O'Leary, B. Chance, and A. G. Yodh, "Scattering of diffuse photon density waves by spherical inhomogeneities within turbid media: analytic solution and applications," Proc. Natl. Acad. Sci. USA **91,** 4887–4891 (1994).
22. O. Axelsson and V. A. Barker, *Finite Element Solution of Boundary Value Problems: Theory and Computation* (Academic, New York, 1984).
23. A. H. Nayfeh and B. Balachandran, *Applied Nonlinear Dynamics: Analytical, Computational, and Experimental Methods* (Wiley, New York, 1995), Chap. 7, Subsec. 7.4.
24. T. M. Griffith, "Temporal chaos in the microcirculation," Cardiovasc. Res. **31,** 342–358 (1996).
25. H. D. I. Abarbanel, R. Brown, J. J. Sidorowich, and L. S. Tsimring, "The analysis of observed chaotic data in physical systems," Rev. Mod. Phys. **65,** 1331–1392 (1993).
26. H. L. Graber, Y. Pei, and R. L. Barbour, "Imaging of spatiotemporal coincident states by dynamic optical tomography," in *Optical Tomography and Spectroscopy of Tissue IV*, B. Chance, R. R. Alfano, B. J. Tromberg, M. Tamura, and E. M. Sevick-Muraca, eds., Proc. SPIE **4250,** 153–163 (2001).
27. R. L. Barbour, H. L. Graber, Y. Pei, and C. H. Schmitz, "Imaging of vascular chaos," in *Optical Tomography and Spectroscopy of Tissue IV*, B. Chance, R. R. Alfano, B. J. Tromberg, M. Tamura, and E. M. Sevick-Muraca, eds., Proc. SPIE **4250,** 577–590 (2001).
28. H. L. Graber, J. Chang, J. Lubowsky, R. Aronson, and R. L. Barbour, "Near infrared absorption imaging of dense scattering media by steady-state diffusion tomography," in *Photon Migration and Imaging in Random Media and Tissues*, B. Chance and R. R. Alfano, eds., Proc. SPIE **1888,** 372–386 (1993).
29. S. R. Arridge, "Optical tomography in medical imaging," Inverse Probl. **15,** 41–93 (1999).
30. G. M. Jenkins and D. G. Watts, *Spectral Analysis and its Applications* (Holden-Day, Oakland, Calif., 1968).
31. J. S. Bendat and A. G. Piersol, *Random Data: Analysis and Measurement Procedures*, 2nd ed. (Wiley, New York, 1986), Chap. 12, Subsec. 12.1.
32. P. Grassberger and I. Procaccia, "Characterization of strange attractors," Phys. Rev. Lett. **50,** 346–349 (1983).
33. R. L. Barbour, H. L. Graber, Y. Pei, S. Zhong, C. H. Schmitz, J. Hira, and I. Arif, "Optical tomographic imaging of dynamic features of dense-scattering media," J. Opt. Soc. Am. A (to be published).
34. More precisely, while certainly there are dynamic-feature measures (e.g., Fourier transform amplitude at a given frequency, magnitude of the cross correlation at a given time lag) whose values *would* be affected by a change in the properties assigned to the reference medium, there also are others [e.g., the frequency at which a peak occurs (or fails to occur) in a Fourier transform map] for which there should be essentially no effect.
35. X. Cheng and D. A. Boas, "Systematic diffuse optical image errors resulting from uncertainty in the background optical properties," Opt. Express **4,** 299–307 (1999), http://www.opticsexpress.org.
36. V. Ntziachristos, B. Chance, and A. G. Yodh, "Differential diffuse optical tomography," Opt. Express **5,** 230–242 (1999), http://www.opticsexpress.org.
37. V. Ntziachristos, A. G. Yodh, M. Schnall, and B. Chance, "Concurrent MRI and diffuse optical tomography of breast after indocyanine green enhancement," Proc. Natl. Acad. Sci. USA **97,** 2767–2772 (2000).
38. A. C. Kak and M. Slaney, *Principles of Computerized Tomographic Imaging* (Institute of Electrical and Electronics Engineers, New York, 1988), pp. 214–218.